A study of the interaction of oxygen with the α_2 phase in the model alloy Ti-7 wt. % Al.

H. M. Gardner[1], A. Radecka[2], D. Rugg[2], D. E. J. Armstrong[1], M. P. Moody[1] and P. A. J. Bagot[1]

1. Department of Materials, University of Oxford, Oxford OX1 3PH, United Kingdom.

2. Rolls-Royce plc, Derby, DE24 8BJ, United Kingdom.

Corresponding Author: hazel.gardner@materials.ox.ac.uk

Abstract

Atom Probe Tomography is used to show that the α_2 phase (Ti_3Al) forms upon ageing Ti-7Al at 550°C with as little as 500 wppm oxygen. Notably, it is found that oxygen consistently partitions away from the α_2 precipitates to the α matrix. The role of aluminium concentration and oxygen solubility on oxygen partitioning preference is also investigated. Based on our observations, we propose a mechanism by which oxygen encourages α_2 formation despite partitioning away from it. Furthermore, nanohardness systematically measured with respect to ageing time and oxygen concentration suggests that α_2 precipitation is not the dominant hardening mechanism during aging.

Keywords: Titanium alloys, α_2 phase, oxygen embrittlement, atom probe tomography, nanoindentation.

Titanium alloys are widely used in the aerospace industry owing to their high specific fatigue strength and good corrosion resistance. For example, fan blades/ discs and compressor blades/ discs in a jet engine are made of titanium alloys such as Ti-6Al-4V and TIMETAL 834.

Even trace amounts of oxygen are known to strengthen, but also embrittle titanium alloys [1–3]. Oxygen encourages formation of the embrittling, ordered α_2 phase (Ti_3Al) during thermal ageing at 500-700°C [4], which is the temperature range experienced during the processing of fan blades. When a load is applied in service to a component containing α_2 precipitates, mobile dislocations travel in pairs through the ordered precipitates. This causes strain localisation, which could make the alloy more susceptible to cold dwell fatigue [5,6].

The effect of oxygen on α_2 formation has been described qualitatively, but the mechanism by which oxygen encourages α_2 precipitation is not fully understood. In this work, the location and quantity of oxygen within the alloy microstructure has been directly measured and related to changes in hardness to provide a better understanding of how oxygen can encourage embrittlement through α_2 formation.

Ti-7 wt. % Al, a model alloy with composition similar to that of the α phase of Ti-6Al-4V fan blade alloy, was supplied by TIMET Witton, Birmingham, UK. The material was melted (using an arc furnace) and controlled amounts of oxygen (500 wppm O or 2500 wppm O) were introduced into the melt via addition of TiO_2 powder. Commercially used α-type titanium alloys often have approximately 800- 2000 wppm O added to provide strength, but this comes at the expense of fracture toughness, especially upon ageing [3,7]. In this study, a range of oxygen concentrations has been selected to investigate how the current, industry-permitted levels of oxygen affect embrittlement.

The material was rolled at 900°C and then recrystallised at 980°C for 1 hour before being quenched in ice water. Samples were then encapsulated under argon and aged for 10 days at 550°C or 49 days at 550°C, respectively. The ageing time has been chosen with the aim of forming α_2, based on the TTT curve for Ti-7Al from Ardakani et al. [4].

Nanoindentation was performed on samples that had been ground using 600-4000 grit SiC paper, polished progressively with 3 µm and 1 µm diamond suspension and then polished with colloidal silica solution neutralised with hydrogen peroxide. 5x5 arrays of 2 µm deep indents, spaced 50 µm apart, were performed with a diamond Berkovich indentor using a NanoIndenterXP (MTS). The contact stiffness was continually measured (2 nm amplitude, 50 Hz oscillation). Hardness and modulus values reported are derived from the CSM data and averaged between depths of 1250-1750 nm, outside the influence of any significant indentation size effects.

Samples for Atom Probe Tomography (APT) were prepared on a Zeiss NVision 40 FIB-SEM (Focussed Ion Beam Scanning Electron Microscope) using the standard lift-out method [8]. APT samples were then analysed with a CAMECA LEAP 5000 HR system, using a laser energy of 40 pJ at a stage temperature of 50 K with a pulse frequency of 200 kHz. APT data analysis was performed using the commercially available Integrated Visualisation and Analysis Software (IVAS, version 3.8.2) package (CAMECA) and the open-access 3Depict software [9]. APT reconstruction was performed using IVAS 3.8.2, using the voltage curve to determine the tip radius.

Aluminium isoconcentration surfaces were generated within the reconstructed APT data to identify the α_2 precipitates. The level of aluminium concentration defining such surfaces was initially varied, and the value which produced the proximity histogram (proxigram) with the narrowest interface width was selected, an approach previously developed by Homma et al. [10]. This was to minimise blurring of the data due to shape misrepresentation. Ions contained within the chosen isoconcentration surface were then extracted as precipitates. The concentration of the extracted precipitates was calculated using a MATLAB mass spectrum peak deconvolution tool [11]. Precipitate volume fraction was estimated by dividing the total number of ions within the precipitates by the total number of ranged ions in the whole APT dataset.

Proxigrams [12] were created from the aluminium isoconcentration surfaces to track change in composition across the precipitate-matrix interface. The mass spectrum peaks contributing to each proxigram bin were then deconvolved using custom Matlab code following the method established by London [13], to provide an accurate composition measurement by accounting for the changing nature of the local mass spectrum as relative position is varied across the interface.

APT reconstructions for each of the aged samples in the Ti-7Al+O series are displayed in figure 1; precipitates were found in the aged samples only. The Ti-Al binary phase diagram [14] does not predict the formation of α_2 for Ti-7Al at 550^{o}C, but the effect of oxygen on the $\alpha/ \alpha + \alpha_2$ boundary must not be neglected. It is known that oxygen reduces the solubility of aluminium in α-titanium, causing the $\alpha/ \alpha + \alpha_2$ boundary to shift to lower aluminium concentrations [3,15–18]. This can be seen more clearly from the Ti-Al-O ternary phase diagram, such as the isothermal section at 600^{o}C [19], which predicts formation of α_2 in Ti-7Al with both 500 wppm O and 2500 wppm O. Comparison of the binary and ternary phase diagram emphasises that both ageing and the addition of oxygen are required to form α_2 in Ti-7Al.

The APT atom maps show that the precipitates formed upon ageing are rich in aluminium, and precipitate compositions are reported in figure 2 (a). It should be noted that the bulk oxygen content of the Ti-7Al + 2500 wppm O, 49 day aged sample, seen in figure 2 (c) is higher than intended; instead of 0.25 wt. % oxygen the sample ultimately contained 0.39 wt. % oxygen. The composition of aluminium in the α_2 precipitates lies within the region of the ternary phase diagram where $\alpha + \alpha_2$ two-phase field is predicted to be stable [19]. Considering the precipitate composition in conjunction with the fact that the Ti-7Al was aged within the α_2 region of the TTT curve [4] provides confidence that the precipitates formed upon ageing are α_2.

Proximity histograms across the precipitate-matrix interfaces in the aged Ti-7Al reveal that oxygen partitions away from the precipitates to the matrix for both oxygen contents and at all ageing times, as seen in figure 3. Ti-7Al is a relatively low aluminium alloy. APT work by Menand et al. [20] shows that for high aluminium alloys such as gamma titanium aluminide, oxygen partitions to the α_2 phase. This suggests that oxygen partitioning preference has some dependence on aluminium concentration.

For high aluminium concentrations (greater than ~ 37 at. % Al) the $\gamma + \alpha_2$ system is stable whereas at lower aluminium concentrations, the $\alpha + \alpha_2$ system is stable. The reported solubility limit of oxygen is highest in the α phase at ~34 at. % [14], dropping to 10-14 at. % in the α_2 phase [21,22] and ~800 at.% ppm in the γ phase [23]. DFT simulations show that oxygen prefers to occupy octahedral interstitial sites that are surrounded by titanium atoms, known as [OTi6] sites [22–26]. Consideration of the number of [OTi6] sites present in each phase can explain the difference in solubility between the γ, α_2 and α phases. One such [OTi6] site exists per atom in the α phase. However, there is only one [OTi6] site per every four atoms in the α_2 phase because, unlike in the α phase, α_2 substitutional sites are not all equivalent due to chemical ordering [23]. Substitution of excess aluminium on the α_2 titanium sites further reduces the number of [OTi6] sites [22]. Oxygen has been observed to fill more interstitial sites than the 50% occupancy that gives rise to maximum configurational entropy, yet fills fewer than the total predicted number of available interstitial sites [22]. This suggests that, as oxygen concentration in the α_2 phase increases, interaction between the interstitial atoms leads to ordering of oxygen on the interstitial sites, reducing the number of [OTi6] sites and limiting the solubility of oxygen in the α_2 phase [22]. In the high aluminium $\gamma + \alpha_2$ system, oxygen is much more soluble in the α_2 phase than the γ phase, due to the small number of [OTi6] sites in the γ phase, and oxygen therefore partitions to the α_2. In contrast, in the $\alpha + \alpha_2$ system, oxygen solubility is higher in the α phase and so oxygen partitions away from the α_2. This is despite the α_2 [OTi6] sites being slightly larger than in α [27]; the effect of the higher number of [OTi6] sites in α outweighs the impact of the [OTi6] site size. Thus, it is proposed that the difference in solubility of oxygen in the phases present is the driving force for oxygen partitioning, and this changes as a function of aluminium content.

Despite oxygen partitioning away from the α_2 phase, it is important to stress that oxygen actually promotes α_2 formation. For example, the α_2 volume fractions in table 1 are consistent with the trend of increasing volume fraction with increasing oxygen content, as reported in the literature for other low aluminium alloys [4,28]. The small volume of material analysed (of the order of $1x10^9$ mm^3 per APT sample) may explain the large standard deviations associated with the measurements. Nevertheless, the broad trend of increasing α_2 volume fraction with oxygen content agrees with previous observations [4,28] that oxygen encourages α_2 formation.

A possible mechanism outlining how oxygen promotes α_2 formation is proposed. As oxygen is added to the α phase, local clustering of aluminium occurs, maximising oxygen solubility by increasing the number of [OTi6] sites. Ordering of these aluminium-rich regions lowers the energy of the system and leads to the formation of the α_2 phase. Thus oxygen reduces the solubility of aluminium in α-titanium, in line with the ternary phase diagram. However, the oxygen is still more soluble in the α phase than the α_2 phase. This results in oxygen subsequently partitioning away from the α_2, even though oxygen initially promotes its formation. This proposed mechanism is consistent with the conditional spinodal mechanism for α_2 formation proposed by Wood et al. [29]. Further work is required to verify this however; for example, measurement of the number of [OTi6] sites as a function of oxygen content in low aluminium titanium alloys could be carried out using neutron diffraction.

Comparison of hardness measurements for just the ice water quenched (IWQ) samples demonstrates that hardness increases with nominal oxygen content. Considering the aged samples, table 1 shows no statistically significant hardness change between the quenched or aged samples with 500 wppm O. However, the Ti-7Al + 2500 wppm O samples do harden significantly upon ageing; ageing for 49 days produces an 8% hardness increase.

In their work on alloys with similar compositions to Ti-64, Liu and Welsch [3] report that α_2 precipitation and intrinsic lattice flow stress have a minor contribution to hardening of the α phase, with solid solution hardening (including solid solution hardening due to interstitial oxygen), work hardening and grain/ phase boundary hardening providing major contributions. At low temperature, ordering of interstitial oxygen atoms in CP-Ti [26] and α- titanium [3,30] can occur, leading to hardening, but ordering is lost at temperatures above 427-577^{o}C [26].

Grain size is comparable across all the samples in this study, as seen in table 2. Average grain size was calculated according to the ASTM E112 intercept procedure [31]. In all cases, the 2 µm indent depth was very much smaller than the grain size, and the indent spacing of 50 µm ensured multiple grains were indented and contributed to the hardness measurement. All samples were recrystallised so should contain very few dislocations. Thus any contributions from work hardening and boundary hardening will be minimal and can be neglected.

Both hardening due to ordering of oxygen and interstitial solid solution hardening could be contributing to the hardness increase between the Ti-7Al + 500 wppm O and Ti-7Al + 2500 wppm O quenched samples. Ageing at 550^{o}C would be expected to lead to a loss of order hardening, as the order-disorder transition temperature is around 427-577^{o}C [26]. However, the hardness remains unchanged between quenching and aging the 500 wppm O material, suggesting that if oxygen ordering is occurring, its effect on hardness is minimal. Other hardening mechanisms that could be acting to increase hardness upon ageing are α_2 precipitation hardening, and increased interstitial solid solution hardening in the matrix due to α_2 causing oxygen to partition to the matrix. Liu and Welsch [3] reported that α_2 precipitation has a minor hardening contribution. The increase from interstitial solid solution hardening is also likely to be small due to the low oxygen content of the material and the corresponding slight difference in oxygen concentration between the precipitate and the matrix. Thus the overall contribution of these hardening mechanisms in the aged 500 wppm O material is likely to be minor.

The same hardening mechanisms (loss of oxygen ordering, α_2 precipitation hardening and interstitial solid solution hardening) could be acting to cause the hardness change upon ageing of the Ti-7Al + 2500 wppm O samples. In contrast to the low oxygen samples, there is a significant 8% increase in hardness upon ageing for the high oxygen samples. The small volume fraction increase from 0.11 to 0.13 between the low and high oxygen 10 day aged samples suggests α_2 precipitation cannot account for the rise in hardness, especially since α_2 precipitation hardening is deemed to be a minor hardness contribution. Thus it seems that interstitial solid solution hardening, which arises due to an increase in matrix oxygen concentration as a result of α_2 formation, is the dominant hardness contribution. From figure 2 (b) it can be seen that, upon ageing, matrix oxygen concentration increases by 200 ppm in the Ti-7Al + 500 wppm O, 10 day aged sample and by 100 ppm in all other aged samples. The Ti-7Al + 2500 wppm O 49 day aged sample is excluded from this, since some external oxygen contamination has occurred.

To directly study the material region which showed the greatest hardness increase, a FIB lift-out was performed from directly beneath an indent in the Ti-7Al+ 2500 wppm O 10 day aged sample, as shown in figure 4. The atom map from this in figure 4 (e) confirms that there are α_2 precipitates

present directly below the indent. However, it seems likely that the α_2 precipitation hardening is providing only a minor contribution to the hardness increase upon ageing. Instead, it is possible that the 100 ppm increase in matrix oxygen content is contributing to the observed 7% hardness increase, which is comparable with the level of interstitial hardening seen in CP-Ti [32,33].

This work highlights that careful control of interstitial oxygen in titanium alloys is necessary as interstitial oxygen plays a significant role in the hardening, and therefore embrittlement of these materials. This research has shown that α_2 precipitation does not contribute significantly to alloy hardening, and a better fundamental understanding of the role of oxygen in its formation has been reached. Further work on the level of oxygen needed to form aluminium clusters, and in different Ti-alloys/processing conditions, would be beneficial to help clarify the mechanism of α_2 precipitation formation.

The authors would like to thank Felicity Dear and Prof. David Dye of Imperial College London for providing samples. EPSRC and Rolls-Royce plc supported the work in this paper under an iCase agreement, project EP/N509711/1.. The EPSRC funded the UK National Atom Probe facility in Oxford under project EP/M022803/1.

References

[1] Q. Yu, R. Traylor, D. Rugg, M. Asta, D.C. Chrzan, A.M. Minor, Science (80-.). 347 (2015) 635–640.

[2] M. Yan, W. Xu, M.S. Dargusch, H.P. Tang, M. Brandt, M. Qian, Powder Metall. 57 (2014) 251–257.

[3] Z. Liu, G. Welsch, Metall. Trans. A 19 (1988) 527–542.

[4] Ardakani, Shollock, Flower, in: Titan. '95 Sci. Technol., 1995.

[5] Z. Wu, C. Qiu, V. Venkatesh, H.L. Fraser, R.E.A. Williams, G.B. Viswanathan, M. Thomas, S. Nag, R. Banerjee, M.H. Loretto, Metall. Mater. Trans. A Phys. Metall. Mater. Sci. 44 (2013) 1706–1713.

[6] A. Radecka, J. Coakley, I.P. Jones, D. Rugg, T.C. Lindley, D. Dye, Mater. Sci. Eng. A 650 (2016) 28–37.

[7] G. Lutjering, J.C. Williams, Titanium, First Edit, Springer, 2003.

[8] K. Thompson, D. Lawrence, D.J. Larson, J.D. Olson, T.F. Kelly, B. Gorman, Ultramicroscopy 107 (2007) 131–139.

[9] D. Haley, Threedepict.Sourceforge.Net, Version 0.0.21 (2010).

[10] T. Homma, A. Arafah, D. Haley, M. Nakai, M. Niinomi, M.P. Moody, Mater. Sci. Eng. A 709 (2018) 312–321.

[11] A. London, Matlab Code, Sourceforge.Net/Projects/Atomprobelab (2019).

[12] B. Gault, M.P. Moody, J.M. Cairney, S.P. Ringer, Atom Probe Microscopy, Springer, 2012.

[13] A.J. London, Microsc. Microanal. 25 (2019) 378–388.

[14] J.L. Murray, Phase Diagrams of Binary Titanium Alloys, ASM International, 1987.

[15] T.K.G. Namboodhiri, C.J. McMahon, H.J. Herman, Metall. Trans. 4 (1973) 1323.

[16] D.J. Truax, C.J. McMahon, Mater. Sci. Eng. 13 (1974) 125–139.

[17] V.V. Vavilova, A.P. Brynza, I.P. Mnuskin, J. Appl. Chem. USSR 48 (1975) 1523–1525.

[18] N. Saunders, in: Titan. '95 Sci. Technol., 1996, p. 2167.

[19] P. (Pierre) Villars, A. Prince, H. (Hiroaki) Okamoto, Handbook of Ternary Alloy Phase Diagrams: Volume 4, ASM International, 1995.

[20] A. Menand, A. Huguet, A. Nérac-Partaix, Acta Mater. 44 (1996) 4729–4737.

[21] K. Das, P. Choudhury, S. Das, J. Phase Equilibria 23 (2002) 525–536.

[22] C.Y. Jones, W.E. Luecke, E. Copland, Intermetallics 14 (2006) 54–60.

[23] W. Lefebvre, A. Loiseau, M. Thomas, A. Menand, Phil Mag A 82 (2002) 2341–55.

[24] S.K. Nayak, C.J. Hung, V. Sharma, S.P. Alpay, A.M. Dongare, W.J. Brindley, R.J. Hebert, Npj Comput. Mater. 4 (2018).

[25] L. Scotti, A. Mottura, J. Chem. Phys 144 (2016).

[26] A. V. Ruban, V.I. Baykov, B. Johansson, V. V. Dmitriev, M.S. Blanter, Phys. Rev. B - Condens. Matter Mater. Phys. 82 (2010) 1–10.

[27] Gehlen, in: R.I. Jaffee (Ed.), Sci. Technol. Appl. Titan., Pergamon Press, 1970.

[28] J.Y. Lim, Metall. Trans. A 7 (1976) 139–144.

[29] H. Wood, G.D.W. Smith, A. Cerezo, Mater. Sci. Eng. A 250 (1998) 83–87.

[30] J.C. Williams, A.W. Sommer, P.P. Tung, Metall. Trans. 3 (1972) 2979–2984.

[31] ASTM, ASTM Stand. E112 Volume 3.1 (2013).

[32] L.P. Lefebvre, E. Baril, Adv. Eng. Mater. 10 (2008) 868–876.

[33] C. Ouchi, H. Iizumi, S. Mitao, Mater. Sci. Eng. A 243 (1998) 186–195.

Figures

Graphical abstract

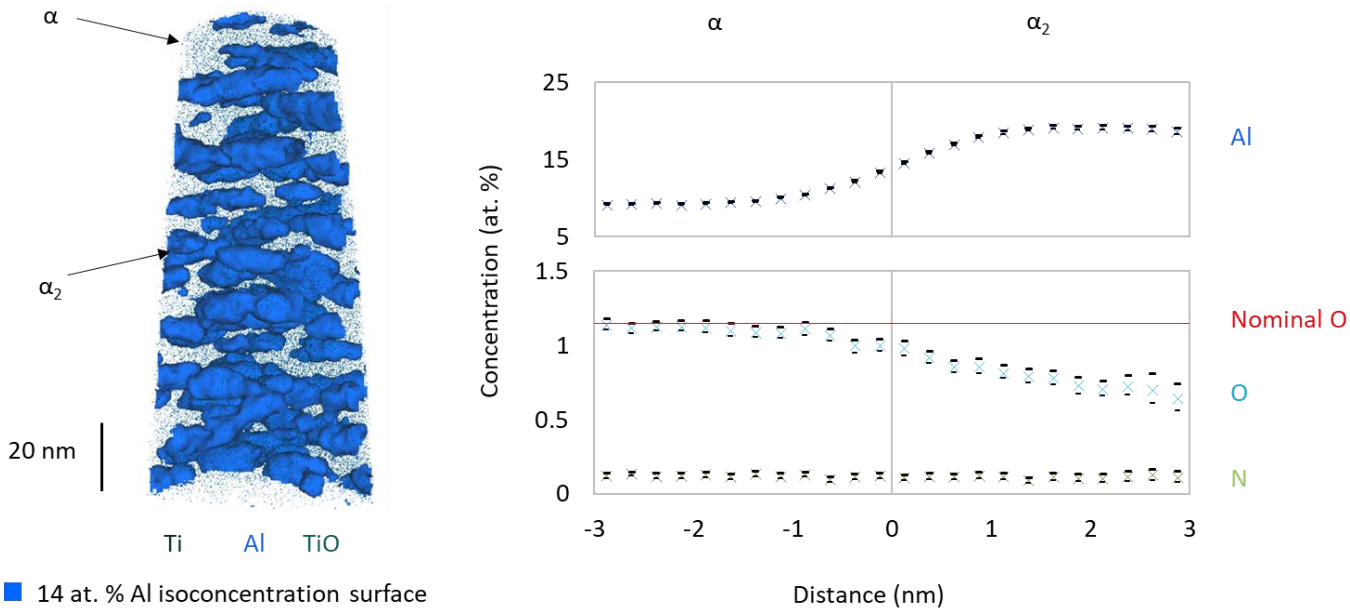

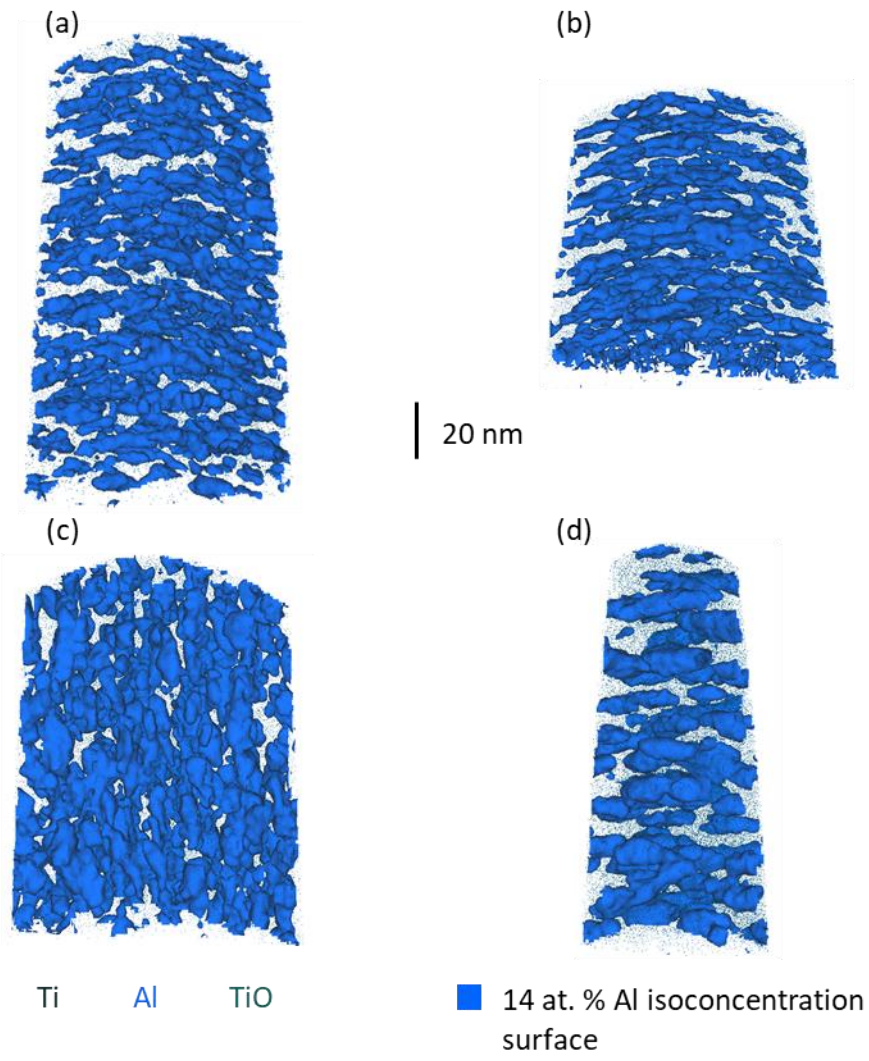

Figure 1: APT atom maps with 14 at. % Al isoconcentration surfaces highlighting α_2 precipitates in (a) Ti-7Al + 500 wppm O, 10 day aged, (b) Ti-7Al + 500 wppm O, 49 day aged, (c) Ti-7Al + 2500 wppm O, 10 day aged and (d) Ti-7Al + 2500 wppm O, 49 day aged (full colour image).

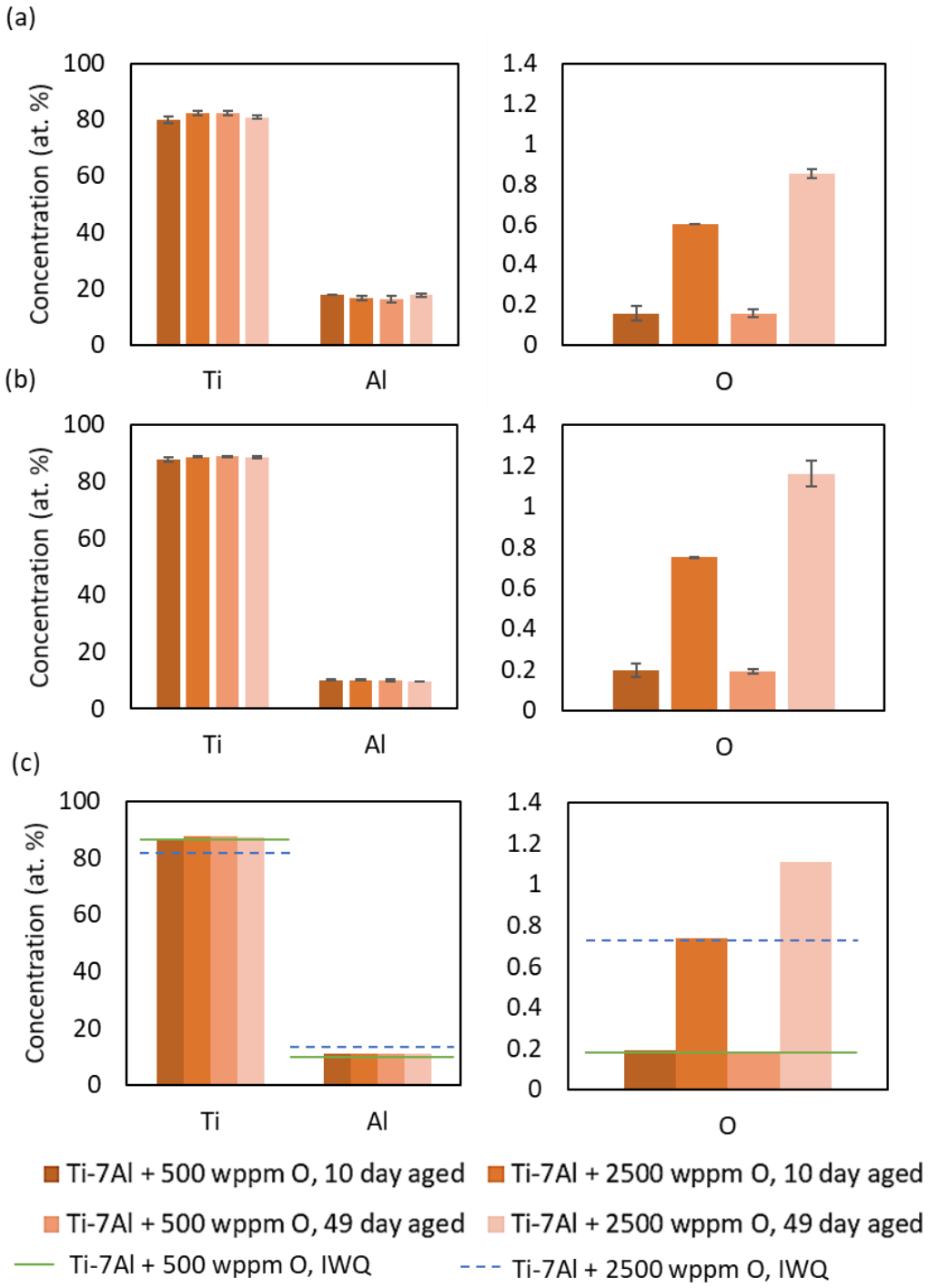

Figure 2: APT-measured compositions of Ti, Al and O in (a) α_2 precipitates, (b) α matrix and (c) bulk material for each of the Ti-7Al samples (full colour image).

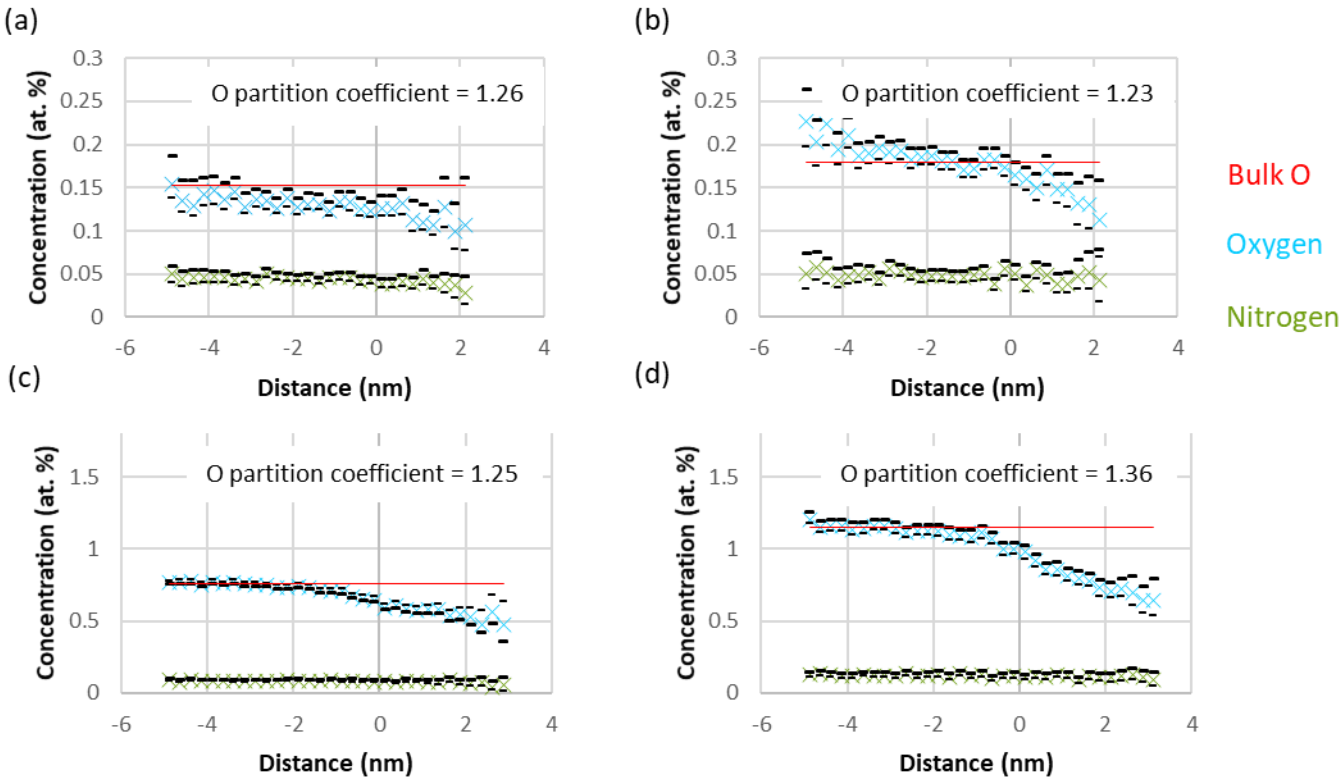

Figure 3: Proximity histograms showing oxygen and nitrogen concentration across the α/ α_2 interface in (a) Ti-7Al + 500 wppm O, 10 day aged, (b) Ti-7Al + 500 wppm O, 49 day aged, (c) Ti-7Al + 2500 wppm O, 10 day aged and (d) Ti-7Al + 2500 wppm O, 49 day aged (full colour image).

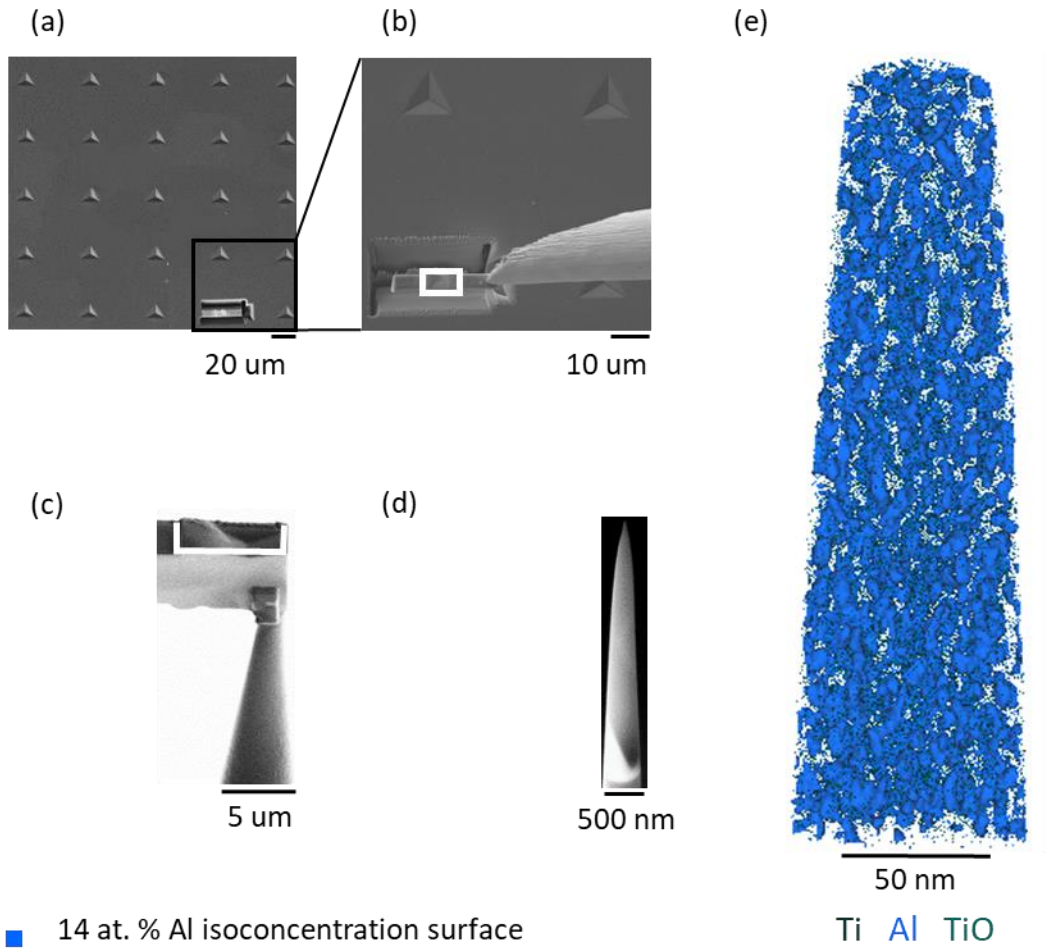

Figure 4: The stages of sample preparation and analysis involved in analysing the material directly below a nanoindent. (a) shows the location of the FIB-milled lift-out bar within the indent array. (b) shows the lift-out bar containing the indent on the end of the micromanipulator. (c) shows the indented material mounted on top of a pre-sharpened silicon post. (d) Shows the indented material sharpened into an APT sample and (e) shows the material analysed in atom probe, containing α_2 precipitates highlighted with 14 at. % Al isoconcentration surfaces (full colour image).